14th International Symposium on Turbulence and Shear Flow Phenomena (TSFP14)
Heidelberg, Germany, July 28–31, 2026

A CONTINUUM FRAMEWORK FOR DENSE SUSPENSIONS FOR THE SIMULATION OF ACTIVE TURBULENCE

H. Ben Gozlen[1,2], **Y. Wang**[1], **M. Oberlack**[1,2]
[1]Chair of Fluid Dynamics, Technical University of Darmstadt, 64287 Darmstadt, Germany
[2]Center for Computational Engineering, Technical University of Darmstadt, 64293 Darmstadt, Germany
bengozlen@fdy.tu-darmstadt.de

Abstract

Collective motion in active suspensions often gives rise to complex, chaotic flow patterns that resemble turbulence on macroscopic scales, despite originating from microscale activity. The significant difference in scale between individual swimmers and entire swarms renders fully resolved simulations computationally intractable, thereby motivating the development of continuum descriptions. To this end, a continuum theory is developed for moderately dense suspensions of active, ellipsoidal particles in an incompressible Newtonian fluid. Starting from the microscale equations that govern fluid and particle motion, a systematic volume averaging procedure yields macroscopic transport equations that link the microscale dynamics to continuum-scale behavior. The resulting two-phase formulation treats the fluid and particle phases as interpenetrating continua with distinct velocities. The particle phase naturally exhibits micropolar behavior, accounting for both translational and independent rotational degrees of freedom. Steric interactions and local alignment are captured through the Oseen-Frank elastic energy, which is incorporated as part of the internal energy of the particle phase. Unclosed terms are systematically closed via thermodynamic arguments, ensuring consistency with the second law of thermodynamics and frame-indifference. The model unifies hydrodynamic and steric interactions, particle anisotropy, and activity within a single continuum framework.

1 Introduction

Active suspensions consist of self-propelled particles that convert internal or environmental energy into mechanical motion, thereby generating active stresses in the surrounding fluid (Bechinger *et al.*, 2016; Ramaswamy, 2017). These systems exhibit rich collective dynamics, including flocking, clustering, and large-scale vortical structures with velocities far exceeding those of individual swimmers (Dombrowski *et al.*, 2004; Koch & Subramanian, 2011). Experimental studies on microorganisms such as *Escherichia coli* and *Bacillus subtilis* have revealed striking examples of such collective motion, including complex, chaotic flow patterns that resemble turbulence on macroscopic scales despite originating from microscale activity. This phenomenon is commonly referred to as *active turbulence* (Mendelson *et al.*, 1999; Cisneros *et al.*, 2011; Koch & Subramanian, 2011).

Unlike classical turbulence, which is driven by inertial instabilities at high Reynolds numbers, active turbulence emerges at vanishingly small Reynolds numbers from the interplay of two classes of interaction: steric interactions, which arise from direct particle contact; and hydrodynamic interactions, which arise from fluid flows generated by each swimmer and influence the motion of others.

Numerous theoretical and computational models have been developed to describe active suspensions. While particle-based approaches (Deußen *et al.*, 2021) can resolve the full coupled fluid-particle dynamics with high fidelity, their computational cost limits the accessible system sizes and time scales. This motivates the development of accurate continuum descriptions. One of the earliest continuum formulations, proposed by Simha & Ramaswamy (2002), adapts the hydrodynamic theory of liquid crystals to active matter and couples it with the Navier-Stokes equations via an active stress tensor representing the collective effect of force dipoles. A more fundamental framework was introduced by Saintillan & Shelley (2008), who developed a kinetic theory for dilute suspensions of self-propelled rods. Their model couples a conservation equation for the orientational distribution of particles with the Stokes equations. Ezhilan *et al.* (2013) later extended this kinetic approach to denser suspensions by incorporating steric alignment effects. However, all of these formulations assume a single shared velocity for the fluid and particle phases. In concentrated suspensions, where drag, lift, and interphase momentum exchange play important roles, this assumption becomes inaccurate. A more realistic approach is to treat the two phases separately within a two-fluid model (Wolgemuth, 2008), which is the strategy adopted in the present work. While Wolgemuth's model introduced separate fluid and particle velocities together with an elastic energy for steric alignment, it was not derived systematically from microscale physics and lacked a thermodynamic closure.

This work adopts the Averaging Theory framework of Anderson & Jackson (1967), originally formulated for passive suspensions of spherical particles, and extends it to ellipsoidal particles with orientation dynamics. The particles are polar in the sense that they possess a vectorial propulsion direction. The averaged equations of continuity, momentum, and energy are derived for both phases. A key finding is that the particle phase exhibits micropolar behavior (Eringen, 1966), accounting for independent particle rotations in addition to translational motion. Steric interactions are captured through the Oseen-Frank elastic energy, and a thermodynamically consistent, frame-indifferent closure is proposed for all unclosed terms. The model is intended for moderately dense suspensions, where frequent collisions generate local orientational order and collective motion. This places it between the dilute limit of independent swimming and the very dense limit where jamming and enduring contact networks dominate.

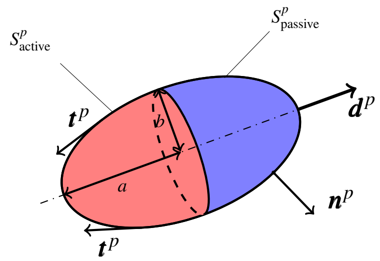

Figure 1. Ellipsoidal Janus particle. The active surface (red) experiences a prescribed tangential stress A_{active} acting along the unit vector $\boldsymbol{t}^p$, while the passive surface (blue) satisfies a no-slip condition. The unit vector $\boldsymbol{d}^p$ denotes the particle orientation along the major axis and $\boldsymbol{n}^p$ the outward surface normal.

2 Microscopic Model

We consider rigid, ellipsoidal Janus particles with a semi-major axis a and equal semi-minor axes b (with an aspect ratio $\lambda = b/a$), which are dispersed in an incompressible Newtonian fluid of density $\hat{\rho}^f$ and viscosity $\hat{\mu}^f$. Each particle p carries an orientation vector d_i^p aligned with its major axis (see Figure 1). The particle Reynolds number satisfies $\mathrm{Re}_p \ll 1$ and the Peclet number $\mathrm{Pe} \gg 1$, so Brownian motion is negligible.

The activity of the particles is modeled using the Janus particle approach, whereby the surface of each particle p is divided into two distinct regions. On the passive surface, denoted by S^p_{passive}, a no-slip boundary condition is imposed

$$u_i^f(\boldsymbol{y}) = u_i^p + \varepsilon_{ijk}\omega_j^p(y_k - y_k^p), \text{ for } \boldsymbol{y} \in S^p_{\text{passive}}, \qquad (1)$$

where u_i^f is the local fluid velocity, u_i^p is the velocity of the particle's center of mass, ω_j^p is its angular velocity, and y_k^p is the position of the particle's center of mass. The convention is adopted that repeated indices are summed over the values one to three.

On the active surface, denoted by S^p_{active}, we prescribe the tangential component of the surface traction in the tangential direction t_i^p. n_i^p is the unit normal vector at the particle surface, pointing from the particle into the fluid. The impermeability condition is enforced in the directions perpendicular to t_i^p. The boundary conditions on the active surface S^p_{active} are

$$\begin{cases} t_i^p \sigma_{ij}^f n_j^p = A_{\text{active}}(\boldsymbol{y}), \\ (\delta_{ij} - t_i^p t_j^p)\left[u_j^f - u_j^p - \varepsilon_{jkl}\omega_k^p(y_l - y_l^p)\right] = 0, \end{cases} \text{for } \boldsymbol{y} \in S^p_{\text{active}}, \qquad (2)$$

where σ_{ij}^f is the fluid stress tensor and $A_{\text{active}}(\boldsymbol{y})$ is the prescribed active traction magnitude.

At the microscopic scale, the fluid motion is governed by the incompressible Navier–Stokes equations:

$$\frac{\partial u_i^f}{\partial y_i} = 0, \quad \hat{\rho}_f\left[\frac{\partial u_i^f}{\partial t} + u_j^f\frac{\partial u_i^f}{\partial y_j}\right] = \frac{\partial \sigma_{ij}^f}{\partial y_j} \qquad (3)$$

subject to the particle boundary conditions (1)–(2). The dynamics of each particle are characterized by the motion of its center of mass and its rotation about this point. Each particle experiences surface tractions exerted by the surrounding fluid and contact forces arising from collisions with neighboring particles. Specifically, when a particle p collides with another particle q, particle q exerts a force $\boldsymbol{f}^{pq}$ and a torque $\boldsymbol{c}^{pq}$ on particle p. The point of application of this interparticle force is denoted by $\boldsymbol{y}^{pq}$. The rigid-body equations of motion for particle p are

$$\hat{\rho}_s v \dot{u}_i^p = \int_{S^p} \sigma_{ij}^f n_j^p \,\mathrm{d}S + \sum_{q\neq p} f_i^{pq} \qquad (4)$$

$$\hat{\Theta}_{ij}\dot{\omega}_j^p = \varepsilon_{ijk}\int_{S^p}(y - y_j^p)\sigma_{kl}^f n_l^p \,\mathrm{d}S + \varepsilon_{ijk}\sum_{q\neq p}(y_j^{pq} - y_j^p) f_k^{pq} + \sum_{q\neq p} c_i^{pq} \qquad (5)$$

where v is the volume of the single particle, $\hat{\rho}_s$ is the particle density and $\hat{\Theta}_{ij}$ its inertia tensor.

3 Volume Averaging

A smooth weighting function $g(\boldsymbol{x},\boldsymbol{y})$, depending only on $|\boldsymbol{y}-\boldsymbol{x}|$, satisfies $\int_V g\,\mathrm{d}^3\boldsymbol{y} = 1$, where $\boldsymbol{y}$ denotes the microscale coordinate and $\boldsymbol{x}$ the macroscale coordinate. The radius of influence ℓ of g is chosen such that $a \ll \ell \ll L$, where L is a characteristic macroscopic length scale. This scale separation ensures that the averaging process is independent of the particular choice of g. The particle volume fraction is defined as

$$\phi(\boldsymbol{x},t) = \int_V \chi(\boldsymbol{y},t)\, g(\boldsymbol{x},\boldsymbol{y})\,\mathrm{d}^3\boldsymbol{y}, \qquad (6)$$

where $\chi(\boldsymbol{y},t)$ is the indicator function of the particle phase. For any microscale field ψ, the fluid-phase and particle-phase averages are defined as

$$(1-\phi)\langle\psi\rangle^f(\boldsymbol{x},t) = \int_V (1-\chi)\,\psi\, g\,\mathrm{d}^3\boldsymbol{y}, \qquad (7)$$

$$n\langle\psi\rangle^p(\boldsymbol{x},t) = \sum_p g(\boldsymbol{x},\boldsymbol{y}^p)\,\psi^p, \qquad (8)$$

where $n(\boldsymbol{x},t) = \sum_p g(\boldsymbol{x},\boldsymbol{y}^p)$ is the particle number density, ψ^p a particle-level property, and $\phi = nv$. Microscale fluid equations are averaged using (7) and microscale particle equations using (8). The key averaging identity for spatial derivatives reads

$$(1-\phi)\left\langle\frac{\partial\psi}{\partial y_i}\right\rangle^f = \frac{\partial}{\partial x_i}\left[(1-\phi)\langle\psi\rangle^f\right] - \sum_p\int_{S^p} g\,\psi\, n_i^p\,\mathrm{d}^2\boldsymbol{y}, \quad (9)$$

with an analogous identity for time derivatives. The surface integrals arising from (9), for example when averaging the force exerted by the particles on the fluid, are expanded in a first-order Taylor series about the particle centre $\boldsymbol{y}^p$. This yields the zeroth and first moments of the fluid-particle interaction force with a truncation error $\mathscr{O}(a^2/L^2)$

$$\sum_p\int_{S^p} g\,\sigma_{ij}^f n_j^p\,\mathrm{d}^2\boldsymbol{y} \approx F_i^f - \frac{\partial S_{ij}^f}{\partial x_j}, \qquad (10)$$

where

$$F_i^f = \sum_p g(\boldsymbol{x}, \boldsymbol{y}^p) \int_{S^p} \sigma_{ij}^f n_j^p \, \mathrm{d}^2\boldsymbol{y}, \tag{11}$$

$$S_{ij}^f = \sum_p g(\boldsymbol{x}, \boldsymbol{y}^p) \int_{S^p} \sigma_{ik}^f n_k^p (y_j - y_j^p) \, \mathrm{d}^2\boldsymbol{y}. \tag{12}$$

4 Macroscopic Equations

Applying the averaging operators to (3)-(5) and using the shorthand of Table 1, the macroscopic balance equations are:
Continuity (both phases):

$$\frac{\partial \rho^\alpha}{\partial t} + \frac{\partial(\rho^\alpha U_i^\alpha)}{\partial x_i} = 0, \quad \alpha \in \{f, p\}. \tag{13}$$

Fluid momentum:

$$\rho^f \frac{\mathrm{d}^f U_i^f}{\mathrm{d}t} = \frac{\partial T_{ij}^f}{\partial x_j} - F_i^f + \frac{\partial S_{ij}^f}{\partial x_j}. \tag{14}$$

Particle momentum:

$$\rho^p \frac{\mathrm{d}^p U_i^p}{\mathrm{d}t} = \frac{\partial T_{ij}^p}{\partial x_j} + F_i^f. \tag{15}$$

Particle angular momentum (micropolar):

$$\rho^p \left(\Theta_{ij} \frac{\mathrm{d}^p \Omega_j^p}{\mathrm{d}t} + \varepsilon_{ijk} \Omega_j^p \Theta_{kl} \Omega_l^p \right) = \frac{\partial M_{ij}^p}{\partial x_j} + \varepsilon_{ijk} T_{kj}^p + \varepsilon_{ijk} S_{kj}^f. \tag{16}$$

Director evolution:

$$\frac{\mathrm{d}^p d_i}{\mathrm{d}t} = \varepsilon_{ijk} \Omega_j^p d_k. \tag{17}$$

The angular momentum equation (16) reveals that the particle phase behaves as a *micropolar fluid*: it possesses an independent macroscopic angular velocity Ω_i^p, which is generally distinct from the fluid vorticity. The director equation (17) follows from the assumption of local alignment, i.e. that neighboring particles are sufficiently aligned so that $d_i(\boldsymbol{x}, t)$ can be treated as an approximately unit vector. This is justified in moderately dense suspensions where orientational order persists on scales much larger than individual particles (Cisneros *et al.*, 2011; Koch & Subramanian, 2011). The terms T_{ij}^f, T_{ij}^p, M_{ij}^p, F_i^f, and S_{ij}^f originate from microscopic fluid tractions and particle contacts and remain unclosed at the macroscale.

5 Internal Energy Equations

The effective specific internal energy of each phase includes thermal and fluctuation contributions. For the fluid phase,

$$\mathscr{E}^f = \langle \varepsilon \rangle^f + \tfrac{1}{2} \langle u_i' u_i' \rangle^f, \tag{18}$$

Table 1. Shorthand notation.

Symbol	Definition
$\rho^f = \hat{\rho}^f(1-\phi)$	fluid partial density
$\rho^p = \hat{\rho}^p \phi$	particle partial density
U_i^f, U_i^p	averaged fluid / particle velocity
Ω_i^p	averaged particle angular velocity
$T_{ij}^f = (1-\phi)\langle \sigma_{ij} \rangle^f - \hat{\rho}^f (1-\phi) \langle u_i' u_j' \rangle^f$	stress tensor of fluid phase
$T_{ij}^p = n \langle s_{ij}^s \rangle^p - \hat{\rho}^p v n \langle u_i' u_j' \rangle^p$	stress tensor of particle phase
$M_{ij}^p = n \langle \mu_{ij}^s \rangle^p - n \langle l_i' u_j' \rangle^p$	couple stress tensor of particle phase
$\Theta_{ij} = \langle \hat{\Theta}_{ij} \rangle^p / (\hat{\rho}^p v)$	averaged inertia tensor

and for the particle phase, translational and rotational fluctuation energies are both included:

$$\rho^p \mathscr{E}^p = \rho^p \langle \varepsilon \rangle^p + \tfrac{1}{2} \rho^p \langle u_i' u_i' \rangle^p + \underbrace{\tfrac{1}{2} n \langle \omega_i \hat{\Theta}_{ij} \omega_j \rangle^p - \tfrac{1}{2} \rho^p \Omega_i^p \Theta_{ij} \Omega_j^p}_{\text{rotational fluctuation energy}}. \tag{19}$$

The effective internal energy equations for each phase follow from the averaged total energy equations by subtracting the averaged kinetic energy equations. The result for the fluid phase is

$$\rho^f \frac{\mathrm{d}^f \mathscr{E}^f}{\mathrm{d}t} = T_{ij}^f \frac{\partial U_i^f}{\partial x_j} - \frac{\partial Q_i^f}{\partial x_i} + \hat{\mathscr{E}}^f, \tag{20}$$

and for the particle phase,

$$\rho^p \frac{\mathrm{d}^p \mathscr{E}^p}{\mathrm{d}t} = -\frac{\partial Q_i^p}{\partial x_i} + T_{ij}^p \left(\frac{\partial U_i^p}{\partial x_j} + \varepsilon_{ijk} \Omega_k^p \right) + M_{ij}^p \frac{\partial \Omega_i^p}{\partial x_j} + \hat{\mathscr{E}}^p, \tag{21}$$

where Q_i^α is the effective heat flux of phase α, and $\hat{\mathscr{E}}^\alpha$ is the inter-phase energy exchange. The sum of the exchange terms can be expressed as

$$\hat{\mathscr{E}}^f + \hat{\mathscr{E}}^p = F_i^f (U_i^f - U_i^p) + (S_{ij}^f)^{\text{sym}} D_{ij}^f + \varepsilon_{ijk} (S_{kj}^f)^{\text{asym}} (\Omega_i^f - \Omega_i^p). \tag{22}$$

Here $D_{ij}^f = \frac{1}{2}(\partial_j U_i^f + \partial_i U_j^f)$ is the fluid rate-of-strain tensor and $\Omega_i^f = \frac{1}{2} \varepsilon_{ijk} \partial_j U_k^f$ is the fluid vorticity vector.

5.1 Oseen-Frank Elastic Energy

Above the critical volume fraction $\phi_{\text{cr}} \approx b/a$, particle collisions generate persistent orientational order described by the director d_i. This threshold corresponds to the point at which each particle has on average at least one neighbor within its effective interaction volume ba^2, making collisions frequent enough to generate persistent orientational correlations and coherent collective motion. The continuum description based on the director field d_i is therefore primarily appropriate in the regime $\phi > \phi_{\text{cr}}$. Spatial distortions of d_i cost energy, modelled by the Oseen-Frank elastic energy $\mathscr{E}_{\text{el}}^p(d_i, \partial_j d_i)$, which satisfies head-tail symmetry $\mathscr{E}_{\text{el}}^p(-d_i, -\partial_j d_i) = \mathscr{E}_{\text{el}}^p(d_i, \partial_j d_i)$. This energy is incorporated as part of the internal energy of the particle phase. The induced elastic stress and couple stress are

$$T^{\mathrm{el}}_{ij} = -\rho^p \frac{\partial \mathscr{E}^p_{\mathrm{el}}}{\partial(\partial_j d_k)} \partial_i d_k, \tag{23}$$

$$M^{\mathrm{el}}_{ij} = \rho^p \varepsilon_{ilk} d_l \frac{\partial \mathscr{E}^p_{\mathrm{el}}}{\partial(\partial_j d_k)}. \tag{24}$$

Including the elastic contribution, the particle energy equation (21) becomes

$$\rho^p \frac{\mathrm{d}^p \mathscr{E}^p}{\mathrm{d}t} = -\frac{\partial Q^p_i}{\partial x_i} + (T^p_{ij} - T^{\mathrm{el}}_{ij})\left(\frac{\partial U^p_i}{\partial x_j} + \varepsilon_{ijk}\Omega^p_k\right) + (M^p_{ij} - M^{\mathrm{el}}_{ij})\frac{\partial \Omega^p_i}{\partial x_j} + \hat{\mathscr{E}}^p. \tag{25}$$

6 Constitutive Theory

The interaction terms F^f_i and S^f_{ij} are decomposed into active and passive contributions. For a constant active stress $A_{\mathrm{active}} = A_0$ on S^p_{active}, analytical integration over the ellipsoidal surface under the assumption of local alignment yields

$$\left(F^f_i\right)_{\mathrm{active}} = -\frac{3\pi A_0 \phi}{8b} d_i, \tag{26}$$

$$\left(S^f_{ij}\right)_{\mathrm{active}} = \frac{A_0 \lambda \phi}{2}\left[d_i d_j - \frac{\lambda^2}{2}(\delta_{ij} - d_i d_j)\right]. \tag{27}$$

The sign of A_0 distinguishes between pushers ($A_0 < 0$), which propel by pushing fluid backwards, and pullers ($A_0 > 0$), which pull fluid forwards. The term (27) is the active stress dipole, which enters the fluid momentum equation (14) through the divergence of S^f_{ij} and drives collective flow in the suspension. This structure is consistent with the active stress tensor introduced by Simha & Ramaswamy (2002) and widely used in kinetic theories (Saintillan & Shelley, 2008; Ezhilan *et al.*, 2013), where it is typically postulated as $\sigma^{\mathrm{active}}_{ij} \propto (d_i d_j - \delta_{ij}/3)$. However, for $A_{\mathrm{active}} \neq$ const, this term cannot be derived directly from the microscale Janus boundary condition by analytical integration, but only numerically.

6.1 Entropy Principle

The passive interaction terms and the stresses are closed using the entropy inequality. Assuming local thermal equilibrium between the phases ($\vartheta^f = \vartheta^p = \vartheta$), introducing the Helmholtz free energy $\Psi^\alpha = \mathscr{E}^\alpha - \vartheta \mathscr{H}^\alpha$, and incorporating the incompressibility constraint

$$(1-\phi)\frac{\partial U^f_i}{\partial x_i} + \phi \frac{\partial U^p_i}{\partial x_i} - \frac{\partial \phi}{\partial x_i}(U^f_i - U^p_i) = 0 \tag{28}$$

via a Lagrange multiplier ζ (Atkin & Craine, 1976), the second law $\vartheta\Pi \geq 0$ yields the full entropy production rate, which decomposes naturally into three contributions: dissipation in the fluid bulk $\vartheta\Pi^f$, dissipation in the particle bulk $\vartheta\Pi^p$, and mechanical dissipation at the fluid-particle interface $\vartheta\Pi^{\mathrm{interface}} = \Pi^{\mathrm{Interface},1} + \Pi^{\mathrm{Interface},2}$,

$$\begin{aligned}\vartheta\Pi = {} & \underbrace{\left[T^f_{ij} + (1-\phi)P^f\delta_{ij}\right]D^f_{ij}}_{\vartheta\Pi^f} \\ & + \underbrace{\left[T^p_{ij} - T^{\mathrm{el}}_{ij} + \phi P^p \delta_{ij}\right]A_{ij} + (M^p_{ij} - M^{\mathrm{el}}_{ij})B_{ij}}_{\vartheta\Pi^p} \\ & + \underbrace{\left[(F^f_i)_{\mathrm{passive}} - P^f \partial_i \phi\right](U^f_i - U^p_i)}_{\vartheta\Pi^{\mathrm{interface},1}} \\ & + \underbrace{(S^f_{ij})^{\mathrm{sym}}_{\mathrm{passive}} D^f_{ij} + \varepsilon_{ijk}(S^f_{kj})^{\mathrm{asym}}_{\mathrm{passive}}(\Omega^f_i - \Omega^p_i)}_{\vartheta\Pi^{\mathrm{interface},2}} \geq 0,\end{aligned} \tag{29}$$

where $A_{ij} = \partial_j U^p_i + \varepsilon_{ijk}\Omega^p_k$ and $B_{ij} = \partial_j \Omega^p_i$. The active interfacial contribution,

$$\vartheta\Pi_{\mathrm{active}} = \left(F^f_i\right)_{\mathrm{active}}(U^f_i - U^p_i) + \left(S^f_{ij}\right)^{\mathrm{sym}}_{\mathrm{active}} D^f_{ij} + \varepsilon_{ijk}\left(S^f_{kj}\right)^{\mathrm{asym}}_{\mathrm{active}}(\Omega^f_i - \Omega^p_i), \tag{30}$$

is excluded from the inequality. The present formulation only resolves the mechanical aspects of active suspensions; the biochemical processes powering particle activity, such as ATP hydrolysis, are not modeled explicitly. Consequently, Π_{active} need not be non-negative, since particles convert chemical free energy into mechanical work rather than dissipating it. In a complete chemo-mechanical framework, the positive entropy production of the underlying chemical reactions would compensate for this, ensuring global compliance with the second law. Since activity is introduced here through prescribed microscale boundary conditions (2), the corresponding macroscopic active terms follow directly from averaging and require no additional thermodynamic closure.

6.2 Equilibrium and Non-Equilibrium Decomposition

At equilibrium, the stresses and couple stress reduce to

$$(T^f_{ij})^{\mathrm{E}} = -(1-\phi)P^f\delta_{ij}, \tag{31}$$

$$(T^p_{ij})^{\mathrm{E}} = -\phi P^p \delta_{ij} + T^{\mathrm{el}}_{ij}, \tag{32}$$

$$(M^p_{ij})^{\mathrm{E}} = M^{\mathrm{el}}_{ij}, \tag{33}$$

where P^f and P^p are the partial pressures. In the dilute limit, where interparticle contacts are negligible, the partial pressures of both phases are equal, $P^f = P^p = P$. In moderately dense suspensions, however, interparticle contacts generate a finite excess pressure in the particle phase that increases with both volume fraction and shear rate. To account for the elevated particle pressure due to interparticle contacts, we adopt the Morris-Boulay model (Morris & Boulay, 1999):

$$P^p = P^f + \hat{\mu}^f K_n \left(\frac{\phi}{\phi_m}\right)^2 \left(\frac{1-\phi}{1-\phi_m}\right)^{-2} \dot{\gamma}^p, \tag{34}$$

where K_n is the dimensionless contact strength, ϕ_m the maximum packing fraction, and $\dot{\gamma}^p = \sqrt{A_{ij}A_{ij}}$ the particle shear rate.

Each field is then decomposed into its equilibrium and dynamic parts:

$$
\begin{aligned}
T_{ij}^{f} &= -(1-\phi)P^{f}\delta_{ij} + (T_{ij}^{f})^{\mathrm{dyn}},\\
T_{ij}^{p} &= -\phi P^{p}\delta_{ij} + T_{ij}^{\mathrm{el}} + (T_{ij}^{p})^{\mathrm{dyn}},\\
M_{ij}^{p} &= M_{ij}^{\mathrm{el}} + (M_{ij}^{p})^{\mathrm{dyn}},\\
(F_{i}^{f})_{\mathrm{passive}} &= P^{f}\partial_{i}\phi + (F_{i}^{f})^{\mathrm{dyn}}_{\mathrm{passive}}.
\end{aligned} \tag{35}
$$

The entropy production rate expressed in dynamic variables is

$$
\begin{aligned}
\vartheta\Pi = \big[(T_{ij}^{f})^{\mathrm{dyn}} + (S_{ij}^{f})^{\mathrm{sym}}_{\mathrm{passive}}\big]D_{ij}^{f} + (T_{ij}^{p})^{\mathrm{dyn}}A_{ij} + (M_{ij}^{p})^{\mathrm{dyn}}B_{ij}\\
+ (F_{i}^{f})^{\mathrm{dyn}}_{\mathrm{passive}}(U_{i}^{f}-U_{i}^{p}) + \varepsilon_{ijk}(S_{kj}^{f})^{\mathrm{asym}}_{\mathrm{passive}}(\Omega_{i}^{f}-\Omega_{i}^{p}) \geq 0.
\end{aligned} \tag{36}
$$

6.3 Constitutive Relations

The entropy inequality (36) imposes constrains on the admissible constitutive relations, but does not uniquely determine their functional form. Three principles govern the closure. First, *phase separation* (Wang & Hutter, 1999): the constitutive relations of each phase depend solely on the kinematic variables of that phase. Second, *frame-indifference*: all constitutive relations must remain invariant under time-dependent rigid rotations of the observer frame, which restricts the tensor structures that may appear. Third, *linear approximation*: each dynamic quantity is expressed as an explicit linear function of the corresponding thermodynamic driving variables, with coefficients that may depend on scalar invariants. This is the simplest physically reasonable choice in the absence of experimental evidence suggesting more complex behavior. The resulting constitutive relations are:

Fluid stress:

$$
(T_{ij}^{f})^{\mathrm{dyn}} = 2\mu^{f}D_{ij}^{f}. \tag{37}
$$

Particle stress:

$$
(T_{ij}^{p})^{\mathrm{dyn}} = \eta_{ijkl}A_{kl}^{\mathrm{sym}} + \Lambda\big[\varepsilon_{ikl}(\tau_{k}^{p})^{\mathrm{dyn}}d_{l}d_{j}\big]^{\mathrm{sym}} - \tfrac{1}{2}\varepsilon_{ijk}(\tau_{k}^{p})^{\mathrm{dyn}}, \tag{38}
$$

$$
(\tau_{i}^{p})^{\mathrm{dyn}} = \gamma_{ij}\big(\hat{\Omega}_{j}^{p} - \Omega_{j}^{p} + \Lambda\varepsilon_{jkl}d_{k}A_{lm}^{\mathrm{sym}}d_{m}\big), \tag{39}
$$

where $\hat{\Omega}_{i}^{p} = \frac{1}{2}\varepsilon_{ijk}\partial_{j}U_{k}^{p}$, $\gamma_{ij} = \gamma_{1}(\delta_{ij}-d_{i}d_{j}) + \gamma_{2}d_{i}d_{j}$, and

$$
\begin{aligned}
\eta_{ijkl} = \eta_{1}\delta_{ij}\delta_{kl} + \eta_{2}(\delta_{il}\delta_{jk} + \delta_{ik}\delta_{jl}) + \eta_{3}(d_{k}d_{l}\delta_{ij} + d_{i}d_{j}\delta_{kl})\\
+ \eta_{4}(d_{i}d_{l}\delta_{jk} + d_{j}d_{k}\delta_{il} + d_{j}d_{l}\delta_{ik} + d_{i}d_{k}\delta_{jl})\\
+ \eta_{5}d_{i}d_{j}d_{k}d_{l}.
\end{aligned} \tag{40}
$$

The general form of η_{ijkl} follows from the representation theory of isotropic tensor functions (Spencer, 1971), applied to a fourth-order tensor depending on the unit vector d_i, together with Onsager reciprocity (Onsager, 1931), which imposes $\eta_{ijkl} = \eta_{klij}$ and reduces the number of independent coefficients. The constitutive relations for the particle stress must additionally be invariant under $d_i \to -d_i$, reflecting the head-tail symmetry of the collision behavior between elongated particles. The effective viscosity of the particle phase is therefore not a scalar but an anisotropic, director-dependent quantity, which gives rise to normal stress differences.

Particle couple stress:

$$
(M_{ij}^{p})^{\mathrm{dyn}} = \beta_{ijkl}^{*}B_{kl}^{\mathrm{sym}} + \beta_{3}\big[\varepsilon_{jil} + \varepsilon_{ikl}d_{k}d_{j} - \varepsilon_{jkl}d_{i}d_{k}\big]\varepsilon_{lmn}\frac{\partial\Omega_{n}^{p}}{\partial x_{m}}, \tag{41}
$$

with $\beta_{ijkl}^{*} = \beta_{1}(\delta_{ij}-d_{i}d_{j})(\delta_{kl}-d_{k}d_{l}) + \beta_{2}[(\delta_{il}-d_{i}d_{l})(\delta_{kj}-d_{k}d_{j}) + (\delta_{ik}-d_{i}d_{k})(\delta_{jl}-d_{j}d_{l})]$. The structure of β_{ijkl}^{*} is chosen to maximize projectors $(\delta_{ij}-d_{i}d_{j})$, reflecting the fact that the component of Ω_{i}^{p} parallel to d_i plays no role in the orientational dynamics.

Interaction terms:

$$
(F_{i}^{f})^{\mathrm{dyn}}_{\mathrm{passive}} = \kappa_{1}(U_{i}^{f}-U_{i}^{p}) + \kappa_{2}\varepsilon_{ijk}(U_{j}^{f}-U_{j}^{p})\varepsilon_{klm}\frac{\partial U_{m}^{f}}{\partial x_{l}}, \tag{42}
$$

$$
(S_{ij}^{f})^{\mathrm{sym}}_{\mathrm{passive}} = \nu_{1}D_{ij}^{f}, \tag{43}
$$

$$
(S_{ij}^{f})^{\mathrm{asym}}_{\mathrm{passive}} = -\nu_{2}\varepsilon_{ijk}(\Omega_{k}^{f}-\Omega_{k}^{p}). \tag{44}
$$

The first term in (42) is the drag force, while the second is a nonlinear lift force that does not contribute to the entropy production rate. However, it is retained as it may become significant in regions of high shear or near walls. Additional contributions, such as Faxén corrections accounting for curvature in the ambient flow field or diffusion-like terms driven by gradients in volume fraction and shear rate, may be incorporated provided consistency with the entropy inequality is verified.

6.4 Thermodynamic Constraints

Substituting the constitutive relations (37)–(44) into the entropy production rate (36) yields

$$
\begin{aligned}
\vartheta\Pi = (2\mu^{f}+\nu_{1})(D_{ij}^{f})^{2} + A_{ij}\alpha_{ijkl}A_{kl} + B_{ij}\beta_{ijkl}B_{kl}\\
+ \kappa_{1}(U_{i}^{f}-U_{i}^{p})^{2} + \nu_{2}(\Omega_{i}^{f}-\Omega_{i}^{p})^{2} \geq 0.
\end{aligned} \tag{45}
$$

Since the entropy production rate attains its minimum, i.e. zero, at thermodynamic equilibrium, the necessary condition for this minimum requires that the second derivative of Π with respect to the thermodynamic driving variables, evaluated at equilibrium, is non-negative definite. This yields the following constraints on the material parameters:

$$
2\mu^{f}+\nu_{1} \geq 0, \quad \kappa_{1} \geq 0, \quad \nu_{2} \geq 0, \tag{46a}
$$

$$
\gamma_{1} \geq 0, \quad \gamma_{2} \geq 0, \quad \eta_{2} \geq 0, \quad \eta_{1}+\eta_{2} \geq 0, \tag{46b}
$$

$$
\eta_{2}+\eta_{4} \geq 0, \quad \eta_{1}+2\eta_{2}+2\eta_{3}+4\eta_{4}+\eta_{5} \geq 0, \tag{46c}
$$

$$
(\eta_{1}+\eta_{2})(3\eta_{2}+4\eta_{4}+\eta_{5}) \geq (\eta_{2}-\eta_{3})^{2}, \tag{46d}
$$

$$
\beta_{2} \geq 0, \quad \beta_{1}+\beta_{2} \geq 0, \quad \beta_{3} \geq 0. \tag{46e}
$$

These inequalities constrain the five viscosity coefficients $\{\eta_i\}$, the two rotational viscosities $\{\gamma_i\}$, the three couple-stress viscosities $\{\beta_i\}$, and the interaction coefficients $\{\kappa_1, \nu_1, \nu_2\}$, providing a complete set of admissibility conditions on the material parameters of the model.

7 Relation To Existing Models

The present framework provides a consistent generalization of the two-fluid model of Wolgemuth (2008). In a two-dimensional periodic domain, neglecting fluid and particle inertia, using a Newtonian (isotropic) closure for the particle stress, excluding dynamic couple stresses ($\beta_i = 0$), retaining elastic contributions only in the angular momentum balance, taking the slender-body limit ($\lambda \ll 1$), and neglecting the Saffman lift force ($\kappa_2 = 0$), the governing equations reduce to the structure of Wolgemuth's model. This confirms that the present formulation recovers known results in the appropriate limit, establishing it as a systematic extension of that model to three dimensions, arbitrary aspect ratio, full micropolar dynamics, and a thermodynamically derived closure.

8 Concluding Remarks

A two-phase, thermodynamically consistent continuum theory has been developed for moderately dense active suspensions of ellipsoidal particles. This work is distinguished by four central contributions.

First, the *micropolar structure* of the particle phase arises naturally from the volume averaging of rigid-body rotation. The director evolution equation follows directly from the averaged angular momentum balance, providing a physically grounded description of rotational dynamics.

Second, *two distinct velocity fields* for the fluid and particle phases are retained, with all fluid-particle interaction terms being explicitly closed. The explicit resolution of relative phase motion enables the model to capture drag, lift, and interphase momentum exchange, all of which become significant at moderate volume fractions.

Third, the *active stress* is derived analytically by directly integrating the Janus boundary conditions over the ellipsoidal surface. This yields explicit expressions for pushers and pullers in terms of the active stress magnitude A_0, the aspect ratio λ, and the volume fraction ϕ.

Fourth, a *thermodynamically consistent closure* is proposed for all unclosed terms. The constitutive relations are derived under the principles of phase separation, frame-indifference, and linearity. The second law of thermodynamics is enforced by requiring the entropy production rate to attain its minimum at equilibrium, yielding explicit admissibility constraints on all material parameters. This provides a systematic and physically consistent basis for the model that does not rely on ad hoc assumptions.

The resulting model reduces to the two-fluid framework of Wolgemuth (2008) in the inertia-free, slender-body, two-dimensional limit, confirming the consistency of the present formulation. The theory is intended for moderately dense suspensions in the regime of frequent but short-lived interparticle collisions ($\phi > \phi_{\text{cr}}$), and is not designed to capture either the dilute limit of independent swimming or the jammed limit, where enduring contact networks dominate. Future work will focus on numerical simulations of representative active suspension configurations to assess the model's predictive capabilities across different geometries and flow regimes.

REFERENCES

Anderson, T. B. & Jackson, R. 1967 Fluid mechanical description of fluidized beds. Equations of motion. *Ind. Eng. Chem. Fundam.* **6**, 527–539.

Atkin, R. J. & Craine, R. E. 1976 Continuum theories of mixtures: Basic theory and historical development. *Q. J. Mech. Appl. Math.* **29**, 209–244.

Bechinger, C., Di Leonardo, R., Löwen, H., Reichhardt, C., Volpe, G. & Volpe, G. 2016 Active particles in complex and crowded environments. *Rev. Mod. Phys.* **88**, 045006.

Cisneros, L. H., Kessler, J. O., Ganguly, S. & Goldstein, R. E. 2011 Dynamics of swimming bacteria: Transition to directional order at high concentration. *Phys. Rev. E* **83**, 061907.

Deußen, T., Wang, Y. & Oberlack, M. 2021 Numerical simulation of active particle suspensions. *Phys. Fluids* **33**, 073303.

Dombrowski, C., Cisneros, L., Chatkaew, S., Goldstein, R. E. & Kessler, J. O. 2004 Self-concentration and large-scale coherence in bacterial dynamics. *Phys. Rev. Lett.* **93**, 098103.

Eringen, A. C. 1966 Theory of micropolar fluids. *J. Math. Mech.* **16**, 1–18.

Ezhilan, B., Shelley, M. J. & Saintillan, D. 2013 Instabilities and nonlinear dynamics of concentrated active suspensions. *Phys. Fluids* **25**, 070607.

Koch, D. L. & Subramanian, G. 2011 Collective hydrodynamics of swimming microorganisms: Living fluids. *Annu. Rev. Fluid Mech.* **43**, 637–659.

Mendelson, N. H., Bourque, A., Wilkening, K., Anderson, K. R. & Watkins, J. C. 1999 Organized cell swimming motions in Bacillus subtilis colonies. *J. Bacteriol.* **181**, 600–609.

Morris, J. F. & Boulay, F. 1999 Curvilinear flows of noncolloidal suspensions: The role of normal stresses. *J. Rheol.* **43**, 1213–1237.

Onsager, L. 1931 Reciprocal relations in irreversible processes. I. *Phys. Rev.* **37**, 405–426.

Ramaswamy, S. 2017 Active matter. *J. Stat. Mech.* p. 054002.

Saintillan, D. & Shelley, M. J. 2008 Instabilities and pattern formation in active particle suspensions: Kinetic theory and continuum simulations. *Phys. Rev. Lett.* **100**, 178103.

Simha, R. A. & Ramaswamy, S. 2002 Hydrodynamic fluctuations and instabilities in ordered suspensions of self-propelled particles. *Phys. Rev. Lett.* **89**, 058101.

Spencer, A.J.M. 1971 *Theory of Invariants*, chap. 3, p. 239–353. Elsevier.

Wang, Y. & Hutter, K. 1999 A constitutive theory of fluid-saturated granular materials and its application in gravitational flows. *Rheol. Acta* **38**, 214–223.

Wolgemuth, C. W. 2008 Collective swimming and the dynamics of bacterial turbulence. *Biophys. J.* **95**, 1564–1574.